Bioimaging **4** (1996) 187–197. Printed in the UK

Avalanche photodiode detection with object scanning and image restoration provides 2–4 fold resolution increase in two-photon fluorescence microscopy

Hiroshi Kano†, Hans T M van der Voort‡, Martin Schrader†, Geert M P van Kempen§ and Stefan W Hell†‖

† Department of Medical Physics and Chemistry, University of Turku, PO Box 123, FIN-20521 Turku, Finland
‡ Scientific Volume Imaging BV, J Geradtsweg 181, NL-1222 PS Hilversum, the Netherlands
§ Pattern Recognition Group, Delft University of Technology, Faculty of Applied Physics, Lorentzweg 1, NL-2628 CJ Delft, the Netherlands

Submitted 6 September 1996, accepted 4 November 1996

Abstract. High-quantum-efficiency photodetection, millisecond pixel dwell time stage scanning and image restoration by maximum-likelihood estimation are synergetically combined and shown to improve the resolution of two-photon excitation microscopy 2–4 fold in all directions. Measurements of the two-photon excitation point-spread function (PSF) of a 1.4 aperture oil immersion lens are carried out by imaging fluorescence beads with a diameter of one seventh of the excitation wavelength (830 nm) and subsequent deconvolution with the bead object function. The proposed method of resolution increase is applied to beads as well as to rhodamine labelled actin fibres in mouse fibroblast cells. As the resolution improvement is not based on the non-linear effect of two-photon excitation, the results imply a comparable resolution increase in single-photon excitation confocal microscopy. In the fibroblasts, we established a three-fold improvement in axial resolution, namely from 840 nm before, to 280 nm after restoration (full-width at half-maximum). Actin fibres with axial distances of 850 nm, otherwise difficult to discern, are fully separated. In the lateral direction, images of fluorescence beads of about 110 nm diameter are restored to the real dimensions of the beads with an accuracy of better than one pixel (41 nm).

Keywords: resolution, fluorescence microscopy, two-photon excitation, avalanche photodiode, high sensitivity, object scanning, restoration, point-spread function, F-actin, mouse fibroblast

1. Introduction

Multiphoton excitation by resonant absorption of two [1] or three photons [2] is a recent development in far-field fluorescence light microscopy. The most prominent advantages of two-photon absorption are the excitation of UV dyes with visible or near-infrared light, three-dimensional imaging without confocal arrangement and superior imaging of strongly scattering specimens [1, 3].

Resonant multiphoton excitation implies the simultaneous absorption of two, three or more photons of an equivalent fraction of energy. A disadvantage encountered with multiphoton resonant excitation is that the comparatively low multiphoton cross sections require high intensities to produce a fluorescence signal that is sufficient for imaging [1–3]. A drawback of lesser importance is that the excitation wavelength, which is 2–3 times longer, leads to a poorer resolution because the non-linearity does not fully

‖ To whom correspondence should be addressed.

0966-9051/96/030187+11$19.50

compensate the adverse effect of the longer wavelength. A confocal pinhole in front of the detector improves the resolution up to that of the corresponding single-photon excitation microscope [4]. The resolution of two-photon excitation microscopy is slightly better when using deep UV dyes for which, in the absence of suitable optical components, the equivalent single-photon excitation is not feasible [1, 5].

The limited signal to noise ratio (SNR) is particularly noteworthy in multiphoton excitation, as the SNR plays a fundamental role in the interpretation of the image. This fact is well known and has been thoroughly discussed in the confocal literature (see [6] for review). A higher SNR increases the information that can be retrieved from a sample. With a noise-free image and a perfectly known point-spread function (PSF), one could locate point objects with arbitrary precision. Despite the considerable progress in this area, far-field fluorescence microscopy is far from reaching this goal. The reasons are that the signal to noise ratio is limited, especially in the high spatial frequency part of the optical transfer function (OTF), which is strongly attenuated due to the asymptotic behaviour of the OTF as it approaches the bandlimit [7]. Furthermore, the PSF is subject to changes induced by optical aberrations and irregularities in the scanning system. Still, an increase in SNR should increase the effective resolution when image restoration techniques are applied [7–14]. One of the goals of this paper is to establish the potential resolution increase by restoration in two-photon fluorescence microscopy.

Restoration techniques have become increasingly useful as faster computers allow for the implementation of stable and more rigorous algorithms [8–14]. For instance, remarkable progress has been reported with conventional CCD microscopy through exploiting an algorithm describing the cell with a continuous object function [13]. Using this method a nearly four-fold improvement in lateral resolution (110 nm at 488 nm excitation wavelength) was reported. This improvement was derived from an intensity decrease of 80% which was found between two adjacent line structures; but as the displayed minimum value is largely represented by a single point, uncertainties in the quantification of this improvement due to (amplified) noise contributions cannot be ruled out. Conventional fluorescence microscopy using a cooled CCD camera has the advantage of parallel imaging which increases the SNR. On the other hand, conventional microscopy lacks an intrinsic axial resolution. This causes, in many situations, the contribution to a voxel value from the in-focus signal to be one or two orders of magnitude smaller than blur contributions. The restoration algorithm must remove the blur contributions and increase the resolution. Small errors in the removal of the large blur component easily result in poor estimates of the in-focus signal. This effect limits the application of conventional restored microscopy to sparse objects where the blur contributions are relatively small. The axial resolution gained by the restoration of conventional microscopes is rather modest, e.g. 400 nm in a computational simulation for highest aperture [13], and possibly lower in a real image.

When using a single lens of highest aperture, the best confocal lateral resolution is about 150–200 nm for single-photon excitation microscopes operating at about 500 nm [6, 15] and 200–250 nm for two-photon excitation microscopes operating in the 750–900 nm region [16]. Both methods feature an intrinsic axial resolution of about 450–650 nm and 650–950 nm, for the single-photon confocal [6] and two-photon [17] methods respectively which facilitates the application of image restoration techniques. On the other hand, image acquisition by scanning reduces the SNR if the total image collection time is fixed, thus counteracting the SNR requirements of a restoration procedure.

In this paper, we optimize far-field two-photon microscopy three-fold. First, we improve the SNR by using a highly sensitive detector. Second, we use an optimized stage scanning microscope in order to reduce aberrations of the PSF [15, 18]. Finally, we apply a maximum-likelihood estimation (MLE) restoration algorithm [14] in order to improve the gain of information and the effective resolution. Because of the intrinsic axial resolution of two-photon microscopy, we expect a considerable increase in effective resolution, especially in the axial direction. We also use a fine pixelation of the order of one tenth of the wavelength in the medium to be able to precisely evaluate a potential resolution increase.

The SNR of a multiphoton excitation microscope is improved by applying a high-quantum-efficiency solid state detector, which in our case, is an avalanche photodiode. While such detectors have been widely used in near-field optics [19] and fluorescence correlation spectroscopy [20], they have, to our knowledge, not been applied effectively in far-field fluorescence imaging. These detectors are considered slow and hence not useful for fast image acquisition. This is, however, less important if the specimen is fixed, the fluorescence signal low, and if morphology rather than functionality is of main concern.

Aberrations of the PSF induced by the objective lens are reduced to a minimum by imaging with a fixed excitation beam that is collinear with the optical axis [15–18]. Scanning of the specimen is accomplished by a piezo stage, and also at a longer recording time. In many respects, the recording conditions of our far-field microscope are similar to those in near-field microscopy [19], thus allowing a comparison of the optical performance of both methods for the (two-photon) fluorescence case.

2. Materials and methods

2.1. Microscope

Figure 1 displays the optical arrangement of the stage scanning two-photon excitation microscope used in the experiments described below. The light source was a mode-locked titanium sapphire laser operating at a wavelength of

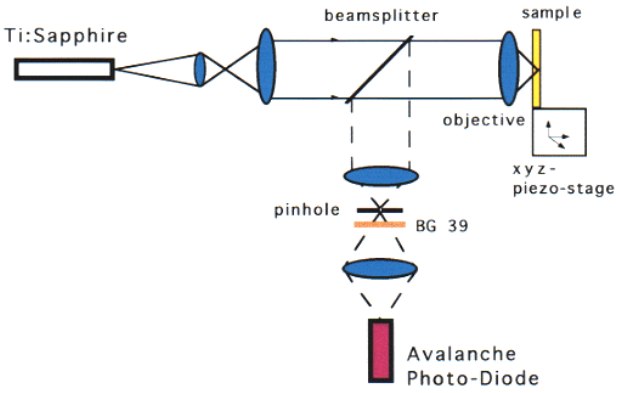

Figure 1. Set-up of the stage scanning two-photon excitation microscope. The fluorescence light passing an oversized pinhole is imaged onto the photosensitive area of an avalanche photodiode.

830 nm. The typical duration of the pulses was about 140 fs in the focal region of the lens [21]. The pulse repetition rate was about 76 MHz. The risk of photobleaching was minimized by operating the microscope at comparatively low power levels. To rule out photobleaching, we illuminated the same site of the sample with the stage fixed over a minute. We observed a stable signal for an average illumination power of the order of 500–1500 μW.

The specimen was mounted on a piezoelectric stage (Melles Griot, Cambridge, UK) positioning the sample with an accuracy of 10 nm in three dimensions. Care was taken to prevent the infrared excitation light from entering the sensitive photodiode. The fluorescence light was separated by a beam splitter and filtered by a blue colour glass (2 mm of BG 39, Schott, Germany). The colour filter suppressed the fluorescence light by about 50%, but the laser was suppressed by nearly 10 orders of magnitude.

The diameter of the pinhole was 100 μm which corresponds to about 3.5 times the back projected Airy disk. Hence our microscope operated in between the confocal and the non-confocal modes. Measurements indicated that this pinhole size is useful because it suppresses both ambient light and, more importantly, lobes in the outer region of the PSF which are due to spherical aberrations of the objective, while preserving most of the fluorescence signal from the main maximum.

The detector was an avalanche photodiode (AQ-121, EG&G Optoelectronics, Canada) operating in the photon counting mode. We determined the average dark signal of the detector as 200 counts per second. The quantum efficiency of these diodes is specified to 25%, 70% and 50% at 400 nm, 633 nm and 830 nm respectively. The light passing through the detector pinhole was projected onto the photosensitive surface of the diode (figure 1).

2.2. Specimens

We used beads and biological samples for our investigations. Beads were used in order to establish the two-photon excitation PSF, as well as the effective resolution for point-like objects after restoration. Mouse fibroblast cells were used for testing the described method in a biological environment. The red fluorescence beads (Molecular Probes, Oregon, USA) had a specified diameter of 120 nm and an absorption maximum at 520 nm. The beads were dispersed on a cover slip and mounted with Aquatex (Merck, Darmstadt, Germany). The index of refraction of Aquatex is 1.395. This index is mismatched with respect to the immersion oil but it is close to that of our biological samples. NIH-3T3 mouse embryonic fibroblasts were grown on cover slips in Dublecco's Modified Eagle's Medium

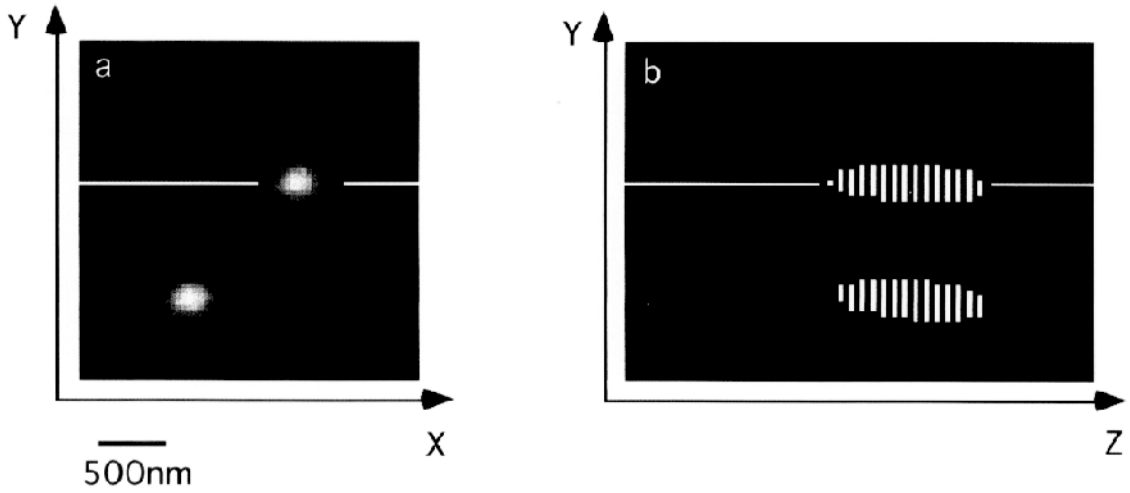

Figure 2. Two-photon image of two 120 nm fluorescence beads, (a) in XY, (b) projection of the data in Z at an intensity threshold of 25%.

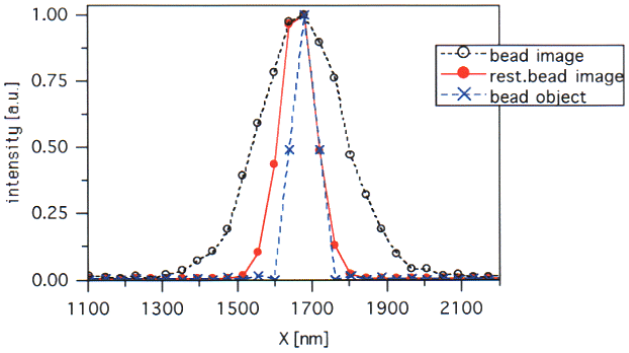

(a)

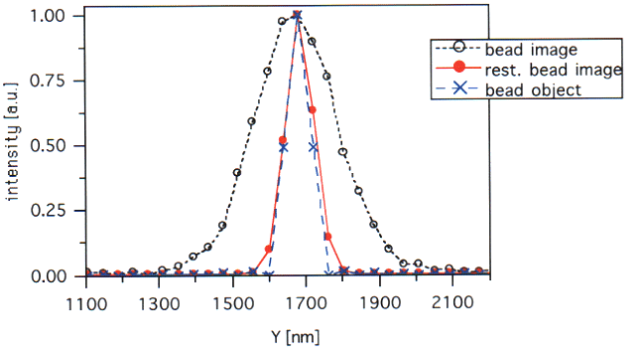

(b)

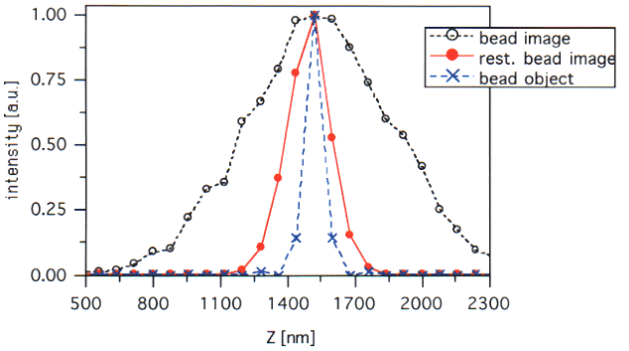

(c)

Figure 3. Profiles in X, Y and Z direction of the bead images, the restored data of the bead and the corresponding profile of an ideal spherical bead object.

(DMEM) supplemented with 5% fetal calf serum (FCS). The fibrous actin (F-actin) of the cells was labelled with rhodamin-conjugated phalloidin (R-415, Molecular Probes Inc., Eugene, OR, USA) [22]. Rhodamine B dissolved in MeOH features a two-photon cross section of 2×10^{-48} s cm^4 at about 830 nm which is about the maximum two-photon cross section for rhodamine B [23]. The cells were mounted using Mowiol 40–88 (Aldrich-Chemie, Steinheim, Germany).

2.3. Restoration algorithm

The aim of the image restoration algorithm was to provide a correction for diffraction effects as well as noise. In fluorescence imaging, the phase of the excitation light is lost upon absorption, so that the image $g(\boldsymbol{r}')$ is given by the convolution of the PSF, $h(\boldsymbol{r})$, with the unknown object function, $f(\boldsymbol{r})$, representing the fluorochrome distribution of the specimen:

$$g(\boldsymbol{r}') = h(\boldsymbol{r}) \otimes f(\boldsymbol{r}) \tag{1}$$

where $\otimes$ denotes the convolution in the object space. Because of the quantal nature of light, the image and the object function are finally determined by noise. At light levels of about 0–200 counts per pixel, the noise obeys a Poisson distribution in a good approximation. We modelled the noise by applying:

$$m(\boldsymbol{r}') = N(g(\boldsymbol{r}')) \tag{2}$$

where $m(\boldsymbol{r}')$ is the recorded image. N is a function accounting for the noise in the signal [14]. The higher spatial frequencies of the optical transfer functions (OTF) of the microscope are suppressed by diffraction and therefore masked by the noise. Thus, a direct inversion of equation (1) is impractical. Instead nearly all restoration schemes use an iterative approach, the main thrust of which is the computation of a new *estimate* of the object function for each iterative step. Iterative restoration algorithms are constructed in such a way that the object estimate convolved with the PSF approaches (matches) the measured image better after each iteration. The criterion used in the matching process largely determines the outcome of the process. The choice of the criterion or distance measure is determined by *a priori* known properties of the object function and the imaging.

An important piece of *a priori* information is that the object function is not negative since it represents a distribution of fluorophores. It has been shown [24] that for non-negative object functions the *I-divergence* distance is the only possible measure that is consistent with a limited set of plausible axioms

$$I(a|b) = a \ln[a/b] - (a - b). \tag{3}$$

The functions a and b are the functions to be compared. Furthermore it is known [25] that minimizing the I-divergence is equivalent to maximizing the logarithmic likelihood, denoted with l, of the estimate f' given the measured image $m(\boldsymbol{r}')$:

$$l(f') = -\int_{R'} g'(\boldsymbol{r}')\,\mathrm{d}\boldsymbol{r} + \int_{R'} \ln[g'(\boldsymbol{r}')]\, m(\boldsymbol{r}')\,\mathrm{d}\boldsymbol{r}' \tag{4}$$

with R' representing the image space and $g'(\boldsymbol{r}')$ the imaged estimate. The function f' which maximizes equation (4) is

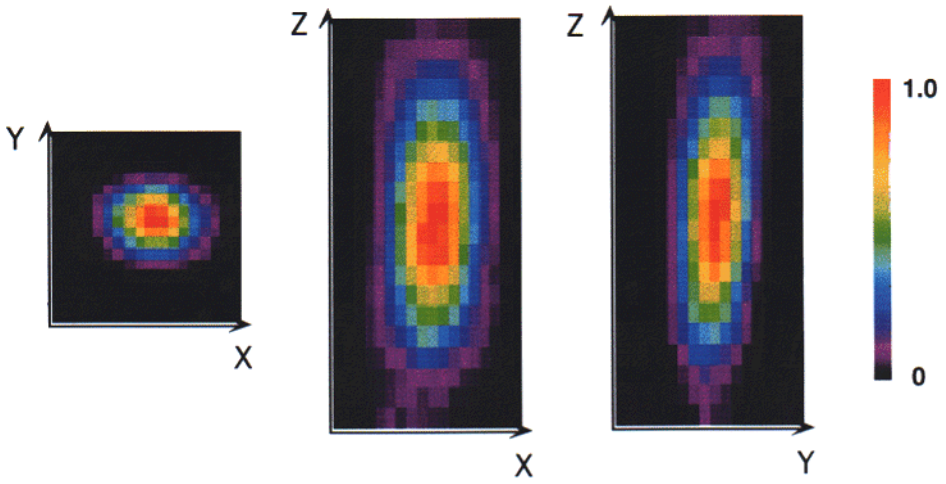

Figure 4. PSF of the two-photon set-up of figure 1; the PSF is obtained from the bead image with subsequent restoration with the bead object function. The pixels represent 40 nm in the lateral direction and 80 nm in the axial direction. The colour bar shows the normalized intensity values.

found with the expectation–maximization algorithm

$$f'^{k+1}(\boldsymbol{r}) = f'^{k}(x)\int_{R'}\left[\frac{h(\boldsymbol{r}-\boldsymbol{r}')}{\int_{R}h(\boldsymbol{r}'-\boldsymbol{r})f'^{k}(\boldsymbol{r})\mathrm{d}\boldsymbol{r}+B}\right]m(\boldsymbol{r}')\,\mathrm{d}\boldsymbol{r}' \tag{5}$$

in which B is a constant background [26–29]. Our choice for the EM–MLE algorithm is motivated by earlier work [14] in which the performance of the EM–MLE algorithm was compared with the widely used iterative constrained Tikhonov–Miller method. It was found that for low light levels, here of the order of 0–200 photons per pixel, the EM–MLE method offers superior performance. The solution found by the EM–MLE algorithm was regularized by the method of Gaussian sieves [30]. In the results shown, a sieve with a sigma of 0.2 sample interval was applied after each fifth iteration of the EM–MLE algorithm. Subsequently, the I-divergence of the imaged estimate and the recorded image was computed and compared to the previous value. The iterations were stopped when the relative change of the I-divergence dropped below 0.01%.

3. Results

3.1. Point-spread-function of the two-photon excitation microscope

First, we determined the PSF of our two-photon excitation microscope by recording 3-D images of fluorescent latex beads. We recorded a stack of 30 parallel XY images that were 80 nm apart in the Z direction. The pixel size in the lateral direction was 41 nm, which is about seven times narrower than the radius of the main focal maximum. These sampling rates amply satisfy the Nyquist criterion. The typical recording time for each layer was 35 s and the pixel dwell time was 2 ms. The maximum number of counts per pixel was 376 in the brightest region. The average illumination power entering the objective lens was 1.5 mW.

Figure 2(a) displays an XY image of two beads with the beads placed in the focal plane of the microscope. To give a feel for the axial extension of the bead image, we have displayed the XZ projection of the XY layers at an intensity threshold of 25%. Hence the parts of the layers with an intensity higher than 25% appear as a bright line (figure 2(b)). The distance between the recorded XY layers was 80 nm. One can recognize the elongation along the optical axis which is due to the poorer resolution in the axial direction. Figures 3(a), (b) and (c) display the lateral and axial profile of the image of the bead in the upper right corner (black dotted line). The ordinate of figure 3(a) and (b) quantifies the counts per pixel and therefore is also a measure for the SNR. At this count level the SNR is mainly determined by shot noise which obeys a Poisson distribution. The ratio of the bead diameter with respect to the wavelength is about one seventh of the excitation wavelength, (110–120 nm versus 830 nm), which is considerably smaller than in other references, e.g. 189 nm versus 488 nm in [13]. One can expect the bead images to be close to the *real* PSF of the two-photon microscope so that the bead image profiles of figure 3 should describe the lateral and axial resolution well.

Despite the small size of the beads, we refined our method and retrieved the real PSF of the microscope from the bead images. We obtained the real PSF by considering the object function of the beads as uniformly dyed 110 nm diameter spheres. A bandlimited object function was generated using the method described in [12]. The PSF determination was performed in much the same way as is approached in a normal regular image restoration

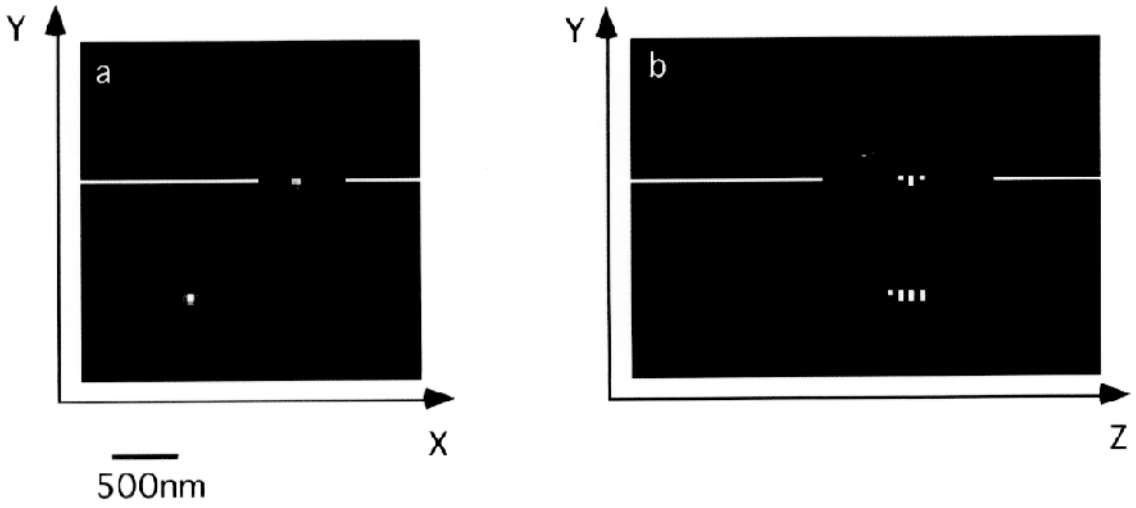

Figure 5. Two-photon image of the restored bead, in (a) XY in the focal plane and in (b) XZ.

procedure. To increase the reliability of the procedure, both beads were used for the evaluation of the real PSF. Because the signal of the combined beads was at least five times stronger than the signal from the biological sample presented here, the sigma of the Gaussian sieve was reduced to 0.1 sample distance (4.1 nm) in the PSF restoration.

The evaluated real PSF is displayed as XY and YZ sections in figure 4. The full-width at half-maximum (FWHM) of the PSF in Z, X and Y was 800 nm, 280 nm and 210 nm, respectively. These values can be regarded as the experimental lateral and axial resolution of our two-photon excitation microscope, prior to restoration. We estimate the statistical errors as ± 20 nm in the axial and ± 10 nm in the lateral direction (1σ).

3.2. Resolution increase for point-like objects with APD-detector stage scanning microscopy and subsequent restoration

With a solution of rhodamine 6G, the fluorescence signal measured with the APD was 12–14 times higher than that measured with the blue-sensitive, photon-counting photomultiplier Hamamatsu R1527, which we routinely used for our investigations [2, 16, 17, 21, 31, 33]. Red sensitive photomultipliers are also as sensitive but are more prone to noise, thus requiring cooling, especially when long integration times are involved. The high SNR and the precise determination of the PSF supports the application of image restoration procedures, such as the MLE algorithm.

As a next step, we applied the real PSF of the system to the 3-D image of the beads of figure 2(a). The background in the restoration algorithm was set to the lowest average value of a 10×10 pixel area in the bottom XY plane of the bead data. The resulting XY and XZ images of the bead are shown in figures 5(a) and (b). The corresponding

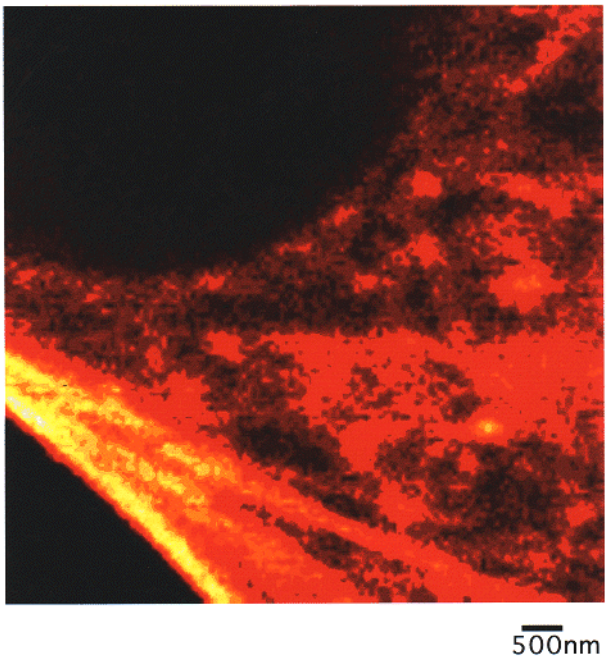

Figure 6. Overview XY image ($10 \times 10\,\mu$m) of the investigated region of the mouse fibroblast. The F-actin filaments are stained with rhodamine-phalloidin.

intensity profiles in the restored bead image are plotted in figure 3 (red solid line). A comparison with the raw data (black dotted line) shows a remarkable sharpening of the bead image.

In order to determine the resolution of our method for point-like objects, one must compare the restored bead images with an ideal object function, namely the ideal profile of a 110 nm solid fluorescence sphere. Hence

the sampled profile of a computed bead is also displayed (blue dashed line). The FWHMs of the image of the bead were 790 nm, 270 nm and 265 nm, and the corresponding restored values were 221 nm, 116 nm, 93 nm, for Z, X and Y, respectively. The FWHM of the bandlimited bead function is 83 nm, and the difference between the restored values and those of the bead are of the order of 10–30 nm which compares well with our accuracy and is below the pixel size.

These results are summarized in table 1. Since the convergence of the restoration procedure depends on the SNR it is important to note that the effective resolution depends both on the SNR as well as on the object to be restored. For point-like objects, such as beads, the resolution improvement is remarkable. It is a result of the synergetic combination of high SNR and optical quality imaging with the MLE-restoration algorithm.

3.3. Imaging of a biological specimen with APD-detector stage scanning microscopy and subsequent restoration

We recorded three-dimensional data sets of the rhodamine B labelled F-actin in the mouse fibroblast cell. Figure 6 shows an XY layer, $10 \times 10\,\mu$m in size, in order to provide an overview of the sample. Figure 7 shows three XY planes of another three-dimensional data stack which has been taken with a smaller pixel size. The size of the images is $2.2 \times 2.2\,\mu$m and the pixel size is 41 nm in the X and Y directions. The axial distance between adjacent XY images in the stack is 80 nm. Here, we show layer numbers 10, 16 and 22 which are equidistant: $Z = 800$ nm, 1280 nm and 1760 nm. We have selected a region of the specimen where the fibres cross each other in different layers. Figure 8 shows an XZ and a YZ slice through the data at $Y = 1394$ nm and at $X = 1927$ nm, respectively.

Table 1. The full-width-at-half-maxima (FWHM) in X, Y and Z direction for the bead images, the restored image, and a solid uniformly stained bead of 110 nm diameter. The restoration is performed by a PSF extracted from two bead images using the maximum-likelihood estimation algorithm.

FWHM	Z (nm)	X (nm)	Y (nm)
bead image	790	270	265
restored bead image	221	116	93
bead object	83	83	83
difference	138	33	10

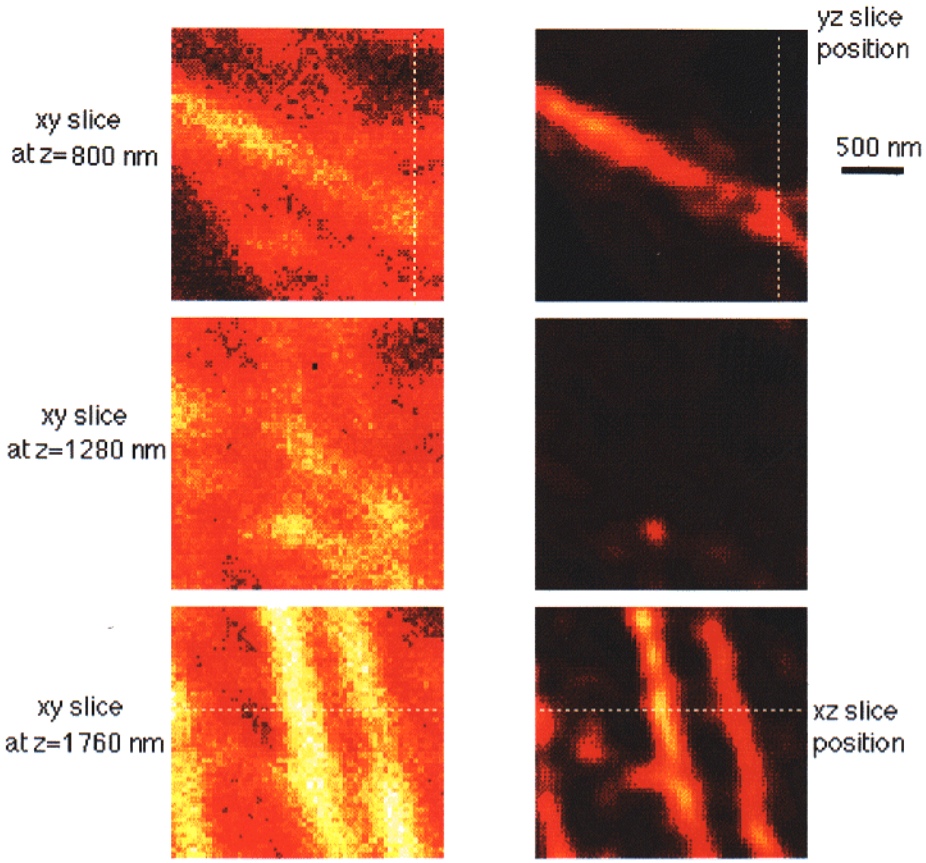

Figure 7. Three XY images of different layers of a 3-D data set of the F-actin in the mouse fibroblast; (left) raw data, (right) after the restoration with the two-photon PSF of figure 4.

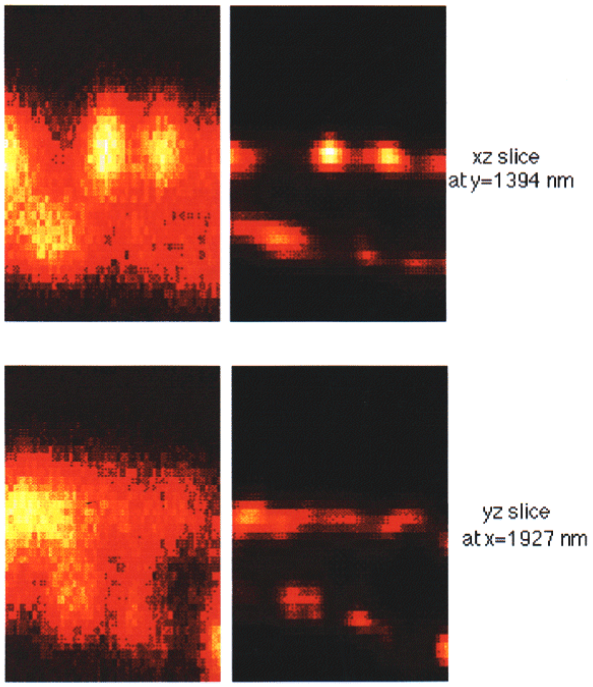

Figure 8. XZ and YZ image of 3-D data set of the F-actin in the mouse fibroblast. Note the improved axial resolution over that of the raw data images.

The image was restored with the PSF as derived with the method described in section 3.1. The background in the restoration algorithm was set to the lowest average value of a 10×10 pixel area in the top XY plane of the fibroblast image.

To provide a feel for the raw data, the images on the left hand side of each pair are *not smoothed*, despite the fact that the pixels are of subresolution dimensions. The images on the right hand side of each pair show the correspondingly restored XY, XZ and YZ images. The XY layer number 22 (at $z = 1760$ nm) is of higher clarity as compared to its unrestored counterpart. Note how the restoration reduces the axial elongation of the focus.

The resolution increase is shown in a comparison of figures 7 and 8 which display typical intensity profiles of the 3-D image before and after the restoration. Figure 9(a) shows the profile of three pronounced F-actin fibres in the X direction. Figure 9(b) shows two adjacent actin fibres in the Y direction and (c) gives a profile in the Z direction. Again the displayed original data was not smoothed, thus providing a feel for the APD stage scanning two-photon imaging at this pixelation. However, restoration also includes smoothing which can be recognized in the restored profiles. The restored profiles have been normalized with respect to the original data so that a direct comparison of the data is possible. Note how in figure 9(b) relatively large values in the left hand side of the raw data profile are not represented in the restored data. The high values in the

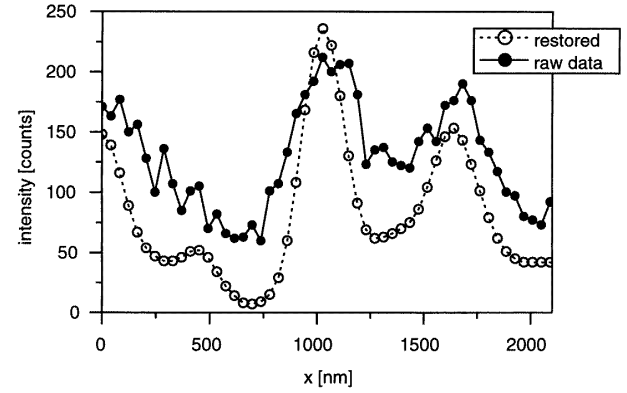

(a)

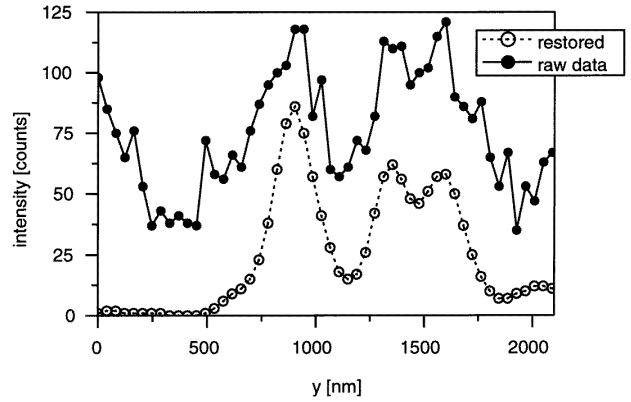

(b)

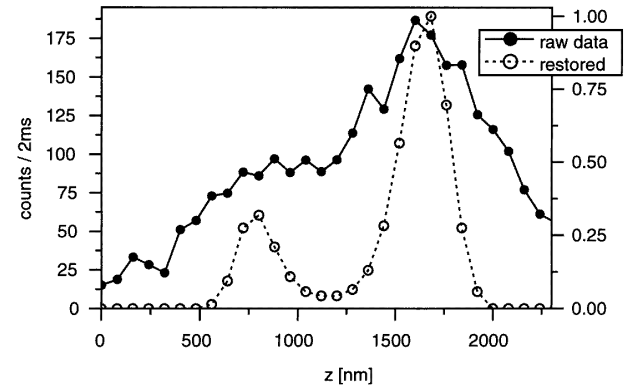

(c)

Figure 9. Raw data profiles and corresponding restored and normalized profiles along the X, Y and Z axis in the data set. The profiles are due to the rhodamine B-labelled actin fibres.

raw data are due to a structure located below the line from which the profile was taken. This structure is just visible in the bottom-right part of the YZ slice shown in figure 8(b).

Figure 10 shows an axial profile with a single fibre. This allows us to estimate the increase in sharpness in fibre imaging in the axial direction. The FWHM of the

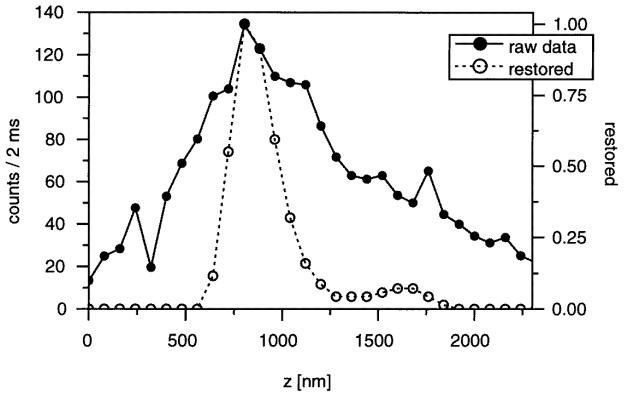

Figure 10. The actin fibre profile before and after restoration quantifies the three-fold increase of axial resolution in the fibroblast cell.

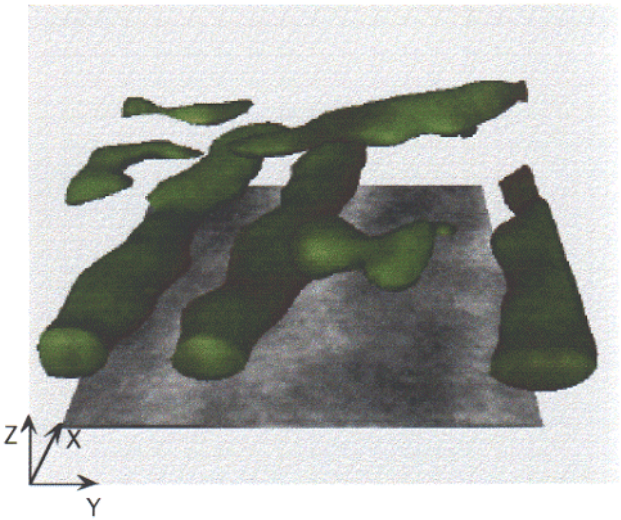

Figure 11. 3-D two-photon restored and rendered image of the labelled f-actin. The 3-D rendering was created with the Imaris 3-D visualization package (Bitplane A G, Switzerland).

unrestored profile is 840 nm, while that of its restored counterpart is 280 nm. This amounts to a resolution increase by a factor of three in axial direction. Figure 11 displays the whole data set in 3-D as a volume rendered object. The actin filaments and the crossing of the F-actin fibres are revealed.

4. Discussion

We have shown that high sensitivity detection combined with high performance far-field optical imaging considerably improves imaging in two-photon fluorescence light microscopy. The combination of high quality data and PSF acquisition with powerful image restoration techniques leads to an improvement in contrast and effective resolution. The gain in effective resolution is readily explained by the additional information in the sample originating from an increased SNR, and the knowledge of the PSF.

For example, we demonstrated that images of point-like fluorescence objects, such as beads, can be restored almost to the real value of the beads in the lateral direction. A remarkable agreement is found between the FWHM of the object and that of the restored bead in the X and Y directions (see table 1). With a difference of 10 nm compared to the FWHM of the object, the image of the bead is virtually restored to the real value of the bead in the Y direction. These results indicate that, with the method proposed in this paper, one should be able to achieve a lateral resolution in the 50–100 nm range for small bright objects. This corresponds to a sharpening of the effective PSF by about 2–4 times in the lateral direction. The results presented in this paper agree well with other results, where we found a lateral FWHM of 40 nm after restoration for point-like, non-fluorescence scatterers [31].

The fact that the restoration did not fully converge to the bead in the X direction can be explained by a slight drift in the scanning of the stage. This drift cannot be fully excluded as the typical recording time, including the dead time, was 35 s per XY plane giving a recording time of a 30 layers stack of 17.5 minutes. This shows that the technique can still be improved and has not reached its limits. Another improvement can be achieved by optimizing the emission filters. Using a dichroic mirror instead of a neutral beam-splitter doubles the signal.

The FWHM of 220–280 nm in the axial direction is about three times narrower than without image restoration. This is a remarkable value for single lens imaging. The axial resolution of point-like objects can also be improved by 4Pi microscopy [4, 32] which primarily uses physical effects for increasing the axial resolution. In addition, collection with two high numerical aperture lenses increases the signal by a factor of 2. Restored 4Pi images of point objects should show an *axial and lateral* resolution of about 50–80 nm in FWHM, i.e. near-isotropic imaging properties. Our results indicate that it should be possible to obtain a resolution of point-like objects such as densely concentrated fluorescence labels of the order of 80–100 nm in a sample. These findings are valuable for the study of a variety of organelles and structures in biology such as the cell nucleus. When expressing the resolution in terms of the wavelength used (here 830 nm) one finds that for beads the resolution is of the order of $\lambda/10$.

What is the relevance of stage scanning in this context? We think that stage scanning provides a PSF that is as spatially invariant as technically possible. Beam scanning can be connected with a PSF that is dependent on the scanning angle of the scanning beam in the entrance pupil of the lens. The invariance of the PSF and also the exact knowledge of the PSF is important for successful restoration (see figures 3, 7, 8), especially when the higher transfer frequencies of the microscope are to be exploited. We think that carefully designed *beam-scanning*

microscopes in conjunction with precise PSF measurements should also reveal an increase in resolution with avalanche photodetectors. It will be interesting to investigate the difference between the two approaches.

When increasing the resolution by image restoration, one must bear in mind that the effective resolution depends on the object [8–12]. For point-like objects, the object function is simple and the convergence of the restoration procedure is more effective. Thus, the resolution of point-like objects is expected to be better than with more structured images. For such cases one can expect considerable potential for application. The restored mouse fibroblasts show an improvement in resolution that is evident both from the 3-D data set as well as from the intensity profiles of figures 9–10. For example, the axial profile of the F-actin fibre is about three times narrower after restoration compared to before. The two fibres in figure 9(c) are separated by 800 nm in the axial direction which is within the FWHM of the two-photon unrestored PSF so that the fibres are not separated in the raw data image. The separation is evident after restoration, as the data feature a pronounced intensity dip of 95% (figure 9(c)) between the two F-actin fibres. The intensity drop is based on several pixels and is a result of the MLE-restoration algorithm.

The improvement of the lateral resolution was more difficult to evaluate, as most of the fibres appeared to be too closely spaced in lateral direction. However, figures 9(a) and (b) demonstrate an improved lateral resolution which we assessed as an improvement by a factor of 1.5–2.0. The improved lateral resolution can be noticed from the more pronounced intensity minima between the structures.

Our results show that avalanche photodiodes are useful for increasing the SNR in scanning fluorescence microscopy. There are two limiting factors that have to be considered with these detectors. The photon counting rate is linear up to a given rate, which was 2 MHz in our case. For a higher rate, some of the photons will be lost leading to a blur of the brighter regions of the image. This should not be a problem with most multiphoton excitation applications as the fluorescence signal is lower. Moreover, avalanche photodetectors are the detectors of choice for multiphoton excited fluorescence in the yellow–red regime, and when long integration times are exploited. In the blue and near-UV wavelength range, photomultipliers also feature a high quantum efficiency and the advantage of photodiodes is not so pronounced. It is also important to bear in mind [6] that the recording time and therefore the SNR cannot be increased without limitation because fluorescence molecules undergo a limited number of excitation–fluorescence cycles before irreversible decomposition. Therefore, increasing the SNR is limited by photobleaching. In our experiments, we have minimized the risk of photobleaching by recording the same site of the specimen 1–3 times and scrutinizing the data for possible signs of photobleaching. The average power values used of about 500–1500 μW are comparatively low in two-photon excitation microscopy [6]. One could also speculate whether slow speed, low intensity two-photon excitation is less damaging to the specimen and to the fluorophore. In our opinion, the determination of ideal parameters for two-photon excitation still deserves attention [33, 34].

Our conclusions also apply to single-photon fluorescence microscopy which often features a better SNR. Hence, with single-photon excitation, the retrievable information and also the resolution should be at least of the order of that reported here. It is also important that the nonlinear nature of two-photon excitation does *not* contribute to the resolution increase described in this paper. In general, as a result of the longer wavelength, two-photon excitation contributes to resolution increase only when comparing the resolution to the excitation wavelength. Two- and three-photon excitation decreases the resolution in absolute numbers. Hence, comparable high-end single-photon excitation microscopy should yield an even better resolution [31]. When the information about the morphology of the sample is more important than imaging speed, the imaging quality as well as the SNR can be improved remarkably. In that sense, our results show that the resolution potential of highly optimized far-field imaging is considerable.

5. Conclusion

We have shown that the imaging and effective resolution of a far-field two-photon excitation fluorescence microscope can be improved by combining high sensitivity detection, precise scanning and PSF determination with restoration techniques. When restoring bead images with an excitation wavelength of 830 nm and a nominal numerical aperture of 1.4 (oil) a lateral effective resolution of the order of 80 nm is achievable; in the axial direction a resolution equal to, or even slightly below 200 nm can be realized. With the FWHM as a reference, this corresponds to resolution improvements by a factor of 3–4 for point-like objects. We have shown a comparable resolution improvement along the optical axis for F-actin fibres in mouse fibroblast cells and a resolution improvement by a factor of 1.5–2 in the lateral direction.

Acknowledgments

The fibroblasts were kindly provided by Diana Toivula, Åbo Akademi University (Turku). HK acknowledges a fellowship by the Japanese Society for the Promotion of Science; MS and SWH acknowledge grants by the European Commission. The restorations were carried out with the Huygens restoration software of Scientific Volume Imaging. Part of this work was conducted in the framework

of a research agreement between SWH and EG&G Wallac Oy (Turku).

References

[1] Denk W, Strickler J H and Webb W W 1990 Two-photon fluorescence scanning microscopy *Science* **248** 73–5

[2] Hell S W, Bahlmann K, Schrader M, Soini A, Malak H, Gryczynski I and Lakowicz J R 1996 Three-photon excitation in fluorescence microscopy *J. Biomed. Opt.* **1** 71–3

[3] Denk W 1996 Two-photon excitation in functional biological imaging *J. Biomed. Opt.* **1** 296–304

[4] Hell S and Stelzer E H K 1992 Fundamental improvement of resolution with a 4Pi-confocal fluorescence microscope using two-photon excitation *Opt. Commun.* **93** 277–82

[5] Gu M and Sheppard C J R 1995 Comparison of three-dimensional imaging properties between two-photon and single-photon fluorescence microscopy *J. Microsc.* **177** 128–37

[6] Pawley J (ed) 1995 *Handbook of Biological Confocal Microscopy* (New York: Plenum)

[7] Goodman J W 1968 *Introduction to Fourier Optics* (New York: McGraw Hill)

[8] Holmes T J, Bhattacharyya S, Cooper J A, Hanzel D, Krishnamurthi V, Lin W, Roysam B, Szarowski D H and Turner J N 1995 Light microscopic images reconstruction by maximum likelihood deconvolution *Handbook of Biological Confocal Microscopy* ed J Pawley (New York: Plenum)

[9] Chen H, Swedlow J R, Grote M, Sedat J W and Agard D 1995 The collection, processing and display of digital and three-dimensional images of biological specimens *Handbook of Biological Confocal Microscopy* ed J Pawley (New York: Plenum)

[10] Shaw P J 1995 Comparison of wide-field/deconvolution and confocal microscopy for 3-D imaging *Handbook of Biological Confocal Microscopy* ed J Pawley (New York: Plenum)

[11] Bertero M, Boccacci P, Brakenhoff G J, Malfanti F and Van der Voort H T M 1990 Three-dimensional image restoration and super-resolution in fluorescence confocal microscopy *J. Microsc.* **157** 3–20

[12] Van der Voort H T H and Strasters K C 1995 Restoration of confocal images for quantitative analysis *J. Microsc.* **178** 165–81

[13] Carrington W A, Lynch R M, Moore E D W, Isenberg G, Fogarty K E and Fay F S 1995 Superresolution three-dimensional images of fluorescence in cells with minimal light exposure *Science* **268** 1483–7

[14] Van Kempen G M P, van der Voort H T M, Bauman J G J and Strasters K C 1996 Comparing maximum likelihood estimation and constrained Tikhonov–Miller restoration *IEEE Eng. Med. Biol.* **15** 76–83

[15] Brakenhoff G J, Blom P and Barends P 1979 Confocal scanning light microscopy with high aperture immersion lenses *J. Microsc.* **117** 219–32

[16] Hänninen P E, Hell S W, Salo J and Soini E 1995 2-photon excitation 4pi confocal microscope—enhanced axial resolution microscope for biological-research *Appl. Phys. Lett.* **66** 1698–700

[17] Hell S W, Hanninen, P E, Kuusisto A, Schrader M and Soini E 1995 Annular aperture 2-photon excitation microscopy *Opt. Commun.* **117** 20–4

[18] Hell S W and Stelzer E H K 1992 Properties of a 4Pi confocal fluorescence microscope *J. Opt. Soc. Am.* A **9** 2159–66

[19] Betzig E, Chichester R J, Lanni F and Taylor D L 1993 Near-field fluorescence imaging of cytoskeletal actin *Bioimaging* **1** 129–36

[20] Rigler R, Widengren J and Mets Ü 1992 Interactions and kinetics of single molecules as observed by fluorescence correlation spectroscopy *Fluorescence Spectroscopy* ed O Wolfbeis (Berlin: Springer)

[21] Hänninen P E and Hell SW 1994 Femtosecond pulse broadening in the focal region of a two-photon fluorescence microscope *Bioimaging* **2** 117–22

[22] Eriksson J E, Paatero G I L, Meriluoto J A O, Codd G A, Nicotera P and Orrenius S 1989 Rapid microfilament reorganization induced in isolated rat hepatocytes by Microcystin-LR, a cyclic peptide toxin *Exp. Cell Res.* **185** 86–100

[23] Xu C and Webb W W 1996 Measurement of 2-photon excitation cross sections of molecular fluorophores with data from 690 to 1050 nm *J. Opt. Soc. Am.* B **13** 481–91

[24] Csiszar I 1991 Why least squares and maximum entropy? An axiomatic approach to inference for linear inverse problems *Ann. Stat.* **19** 2032–66

[25] Snyder D L, Schutz T J and O'Sullivan J A 1992 Deblurring subject to nonnegative constraints *IEEE Trans. Signal Proces.* **40** 1143–50

[26] Dempster A P, Laird N M and Rubin D B 1977 Maximum likelihood from incomplete data via the EM algorithm *J. R. Stat. Soc.* B **39** 1–37

[27] Shepp L A and Vardi Y 1982 Maximum likelihood reconstruction for emission tomograpy *IEEE Trans. Med. Imag.* **MI-1** 113–21

[28] Richardson W H 1972 Bayesian-based iterative method of image restoration *J Opt. Soc. Am.* **62** 55–9

[29] Lucy L B 1974 An iterative techniquefor the rectification of observed distributions *Astron. J.* **79** 745–54

[30] Snyder D L, Hammoud A M and White R L 1993 Image recovery from data acquired with a charge-coupled-device camera *J. Opt. Soc. Am.* **10** 1014–23

[31] Schrader M, Hell S W and van der Voort H T M 1996 Potential of confocal microscopes to resolve in the 50–100 nm range *Appl. Phys. Lett.* **69** 3641–3

[32] Schrader M and Hell S W 1996 4Pi-confocal images with axial superresolution *J. Microsc.* **183** 189–93

[33] Hänninen P E, Schrader M, Soini E and Hell S W 1995 Two-photon excitation fluorescence microscopy using a semiconductor laser *Bioimaging* **3** 70–75

[34] Brakenhoff G J, Müller M and Ghauharali R I 1996 Analysis of efficiency of two-photon versus single-photon absorption for fluorescence generation in biological objects *J. Microsc.* **183** 140–4